



Article

# Influence of Magnetic Nanoparticles on Modified Polypyrrole/*m*-Phenylenediamine for Adsorption of Cr(VI) from Aqueous Solution

Thabiso Carol Maponya <sup>1</sup>, Kabelo Edmond Ramohlola <sup>1</sup>, Nazia Hassan Kera <sup>2</sup>,  
Kwena Desmond Modibane <sup>1,\*</sup> , Arjun Maity <sup>2</sup>, Lebogang Maureen Katata-Seru <sup>3</sup>  and  
Mpitloane Joseph Hato <sup>1,4,\*</sup>

<sup>1</sup> Nanotechnology Research Lab, Department of Chemistry, School of Physical and Mineral Sciences, University of Limpopo (Turfloop), Sovenga 0727, Polokwane, South Africa; 2209thabiso@gmail.com (T.C.M.); kabelo.ramohlola@ul.ac.za (K.E.R.)

<sup>2</sup> DST/CSIR Innovation Centre, National Centre for Nanostructured Materials, CSIR Material Science and Manufacturing, Pretoria 0001, South Africa; Kera.Nazia@csir.co.za (N.H.K.); AMaity@csir.co.za (A.M.)

<sup>3</sup> Chemistry Department, Faculty of Natural and Agricultural Sciences, North-West University, Mmabatho 2735, South Africa; Lebo.Seru@nwu.ac.za

<sup>4</sup> Department of Environmental Sciences, College of Agriculture and Environmental Sciences, University of South Africa (UNISA), Florida Science Campus, Johannesburg 1710, South Africa

\* Correspondence: kwena.modibane@ul.ac.za (K.D.M.); mpitloane.hato@ul.ac.za (M.J.H.)

Received: 21 January 2020; Accepted: 20 February 2020; Published: 19 March 2020



**Abstract:** A novel, modified polypyrrole/*m*-phenylenediamine (PPy-*m*PD) composite, decorated with magnetite (Fe<sub>3</sub>O<sub>4</sub>) nanoparticles, and prepared via an in-situ oxidative polymerisation, was investigated. The PPy-*m*PD/Fe<sub>3</sub>O<sub>4</sub> nanocomposite was employed for the removal of highly toxic oxyanion hexavalent chromium Cr(VI) from an aqueous solution. The structure and successful formation of the PPy-*m*PD/Fe<sub>3</sub>O<sub>4</sub> nanocomposite was confirmed and investigated using various techniques. The presence of Fe<sub>3</sub>O<sub>4</sub> was confirmed by high resolution transmission electron microscopy, with an appearance of Fe lattice fringes. The estimation of the saturation magnetisation of the nanocomposite, using a vibrating sample magnetometer, was observed to be 6.6 emu/g. In batch adsorption experiments, PPy-*m*PD/Fe<sub>3</sub>O<sub>4</sub> nanocomposite (25 mg) was able to remove 99.6% of 100 mg/L of Cr(VI) at pH 2 and 25 °C. Adsorption isotherms were investigated at different Cr(VI) concentration (100–600 mg/L) and temperature (15–45 °C). It was deduced that adsorption follows the Langmuir model, with a maximum adsorption capacity of 555.6 mg/g for Cr(VI) removal. Furthermore, isotherm data were used to calculate thermodynamic values for Gibbs free energy, enthalpy change and entropy change, which indicated that Cr(VI) adsorption was spontaneous and endothermic in nature. Adsorption–desorption experiments revealed that the nanocomposite was usable for two consecutive cycles with no significant loss of adsorption capacity. This research demonstrates the application potential for the fascinating properties of PPy-*m*PD/Fe<sub>3</sub>O<sub>4</sub> nanocomposite as a highly efficient adsorbent for the removal of heavy metal ions from industrial wastewater.

**Keywords:** water pollution; *m*-phenylenediamine; magnetic polymer nanocomposite; kinetics; adsorption properties

## 1. Introduction

Water is the life artery of living systems that is essential to human health and welfare, and a prerequisite to industrial development. Millions of people in the world are estimated to die each year as a result of unsafe drinking water [1]. For this reason, wastewater treatment is essential to the safety

of human beings. The removal of toxic heavy metals, such as lead (Pb), cadmium (Cd), chromium (Cr) and copper (Cu), is one of the main problems for wastewater treatment [2].

These pollutants can enter water systems through industrial mining, galvanoplastic foundries, and from pipe corrosion. Therefore, a long-term exposure to these heavy metals can accumulate in living organisms, causing several disorders and serious diseases [2]. Thus, it is important to search for economical and efficient methods to protect water resources from pollution.

Polypyrrole (PPy) is a conducting polymer that has been studied to remove hexavalent chromium from water, due to its fascinating properties, such as its ease of chemical substitution, high chemical stability, ion exchange behaviour, and the ability to reduce toxic Cr(VI) to less toxic Cr(III) [1–5]. A number of studies have reported on the functionalisation of PPy to increase the number of amine functional groups, which can facilitate chelation or adsorption of Cr(VI) ions by serving as adsorption sites for Cr(VI) [4,6,7]. For example, polyacrylonitrile/polypyrrole (PAN/PPy) core-shell-structured nanofibers synthesised via the electrospinning technique for the removal of Cr(VI) with an adsorption capacity of 61.80 mg/g, was reported [6]. Kera et al. [2], synthesised a PPy/2,5-diaminobenzene sulfonic acid (DABSA) composite via an in-situ oxidative polymerisation of PPy in the presence of DABSA. The PPy/DABSA composite had an adsorption capacity of 303 mg/g at 25 °C. In another study, PPy-*m*-phenylenediamine (*m*PD) with a high adsorption capacity of 526 mg/g for Cr(VI) at 25 °C and initial pH 2, was reported [2]. The incorporation of *m*PD resulted in an increase in the number of amine functional groups and active sites for Cr(VI) uptake, and significantly enhanced the surface area of PPy. In all these studies, it has been realised that the application of PPy-based composite adsorbents for water treatment is challenging, owing to difficulties in separating these adsorbents from the aqueous media after an adsorption process [7–9]. Therefore, the magnetic separation process has been one of the most employed techniques to circumvent the separation problem of adsorbents from aqueous solutions [10]. Magnetic nanoparticles, such as maghemite ( $\gamma$ -Fe<sub>2</sub>O<sub>3</sub>), magnetite (Fe<sub>3</sub>O<sub>4</sub>) [11–13] and Jacobsite (MnFe<sub>2</sub>O<sub>4</sub>) [14,15], have received much attention to assist during the magnetic separation process, due to their large surface areas and good water dispersion ability [16]. In addition, these nanoparticles are advantageous for the adsorption process, because of their high surface to volume ratio, resulting in a higher adsorption capacity for metal removal compared to other materials [2,10,16].

A number of studies have been carried out using magnetic PPy-based nanocomposites for the adsorption of Cr(VI) from wastewater [2,10,17]. PPy decorated with reduced graphene oxide (rGO)-Fe<sub>3</sub>O<sub>4</sub> composite with an adsorption capacity of 293.3 mg/g was reported [18]. PPy/Fe<sub>3</sub>O<sub>4</sub> and PPy-PANI/Fe<sub>3</sub>O<sub>4</sub> nanocomposites were synthesised for the removal of Cr(VI) by various researchers [2,8]. The authors found that the PPy/Fe<sub>3</sub>O<sub>4</sub> and PPy-PANI/Fe<sub>3</sub>O<sub>4</sub> nanocomposites showed adsorption capacities of 196.4 and 303 mg/g for Cr(VI) removal at pH 2 and 25 °C, respectively.

The aim of this study was to synthesise a highly effective PPy-*m*PD/Fe<sub>3</sub>O<sub>4</sub> nanocomposite adsorbent by a simple in-situ oxidative polymerisation route for the adsorption of Cr(VI) from water. It is reported that the presence of *m*PD in the nanocomposite enhanced the adsorption capacity of the PPy [3]. Herein, Fe<sub>3</sub>O<sub>4</sub> nanoparticles were incorporated into the PPy-*m*PD composite to enhance its Cr(VI) adsorption capacity, and to simplify the separation of the adsorbent from the aqueous solution after the adsorption process. The synthesised PPy-*m*PD/Fe<sub>3</sub>O<sub>4</sub> nanocomposite was studied as an adsorbent for the removal of Cr(VI) from wastewater in batch-type experiments.

## 2. Experimental

### 2.1. Materials

Pyrrole monomer (Py) (98%), iron chloride (FeCl<sub>3</sub>), magnetite (Fe<sub>3</sub>O<sub>4</sub>) nanoparticles, *m*-phenylenediamine (*m*PD) and 1,5-diphenylcarbazine were purchased from Sigma-Aldrich (South Africa). Potassium dichromate (K<sub>2</sub>Cr<sub>2</sub>O<sub>7</sub>) was obtained from Minema Chemicals (Johannesburg, South Africa). Cr(VI) stock solution (1000 mg/L) was prepared by dissolving a pre-determined amount of K<sub>2</sub>Cr<sub>2</sub>O<sub>7</sub> in deionised water. Py was distilled under vacuum for purification and stored in the

refrigerator until used. Other chemicals used in this study were of analytical grade, and were used as received.

### 2.2. Synthesis of PPy-*m*PD/Fe<sub>3</sub>O<sub>4</sub> Nanocomposite

PPy-*m*PD/Fe<sub>3</sub>O<sub>4</sub> nanocomposite was prepared via the in-situ polymerisation of pyrrole and *m*PD monomers in the presence of Fe<sub>3</sub>O<sub>4</sub>, according to the method reported by Kera et al. [3]. Typically, Fe<sub>3</sub>O<sub>4</sub> (0.05 g) was uniformly dispersed in 100 mL of deionised water by ultrasonication for 30 min. The magnetite solution was allowed to cool down to room temperature, and 0.8 g of *m*PD was added to the mixture and dissolved by shaking. Py monomer, 0.8 mL, was then transferred into the mixture, which was agitated to disperse the Py uniformly. FeCl<sub>3</sub> solution was prepared in a separate container by dissolving 6 g of FeCl<sub>3</sub> in 100 mL of deionised water. The FeCl<sub>3</sub> solution was then transferred into the mixture all at once, and agitated by shaking for 10 min at room temperature. The reaction mixture was left for 24 h for the polymerisation process to take place. The black resultant precipitate was obtained from the reaction mixture through filtration and was washed with deionised water and acetone to obtain a colourless filtrate. Then, the product was dried at 60 °C for 24 h under vacuum (mass obtained = 1.12 g).

### 2.3. Characterisations

The elemental analysis, morphology, and mapping of the PPy homopolymer and PPy-*m*PD/Fe<sub>3</sub>O<sub>4</sub> nanocomposite before and after Cr(VI) adsorption were studied by using field-emission scanning electron microscopy (FE-SEM) (Auriga Cobra focused-ion beam FIB-SEM, Carl Zeiss, Jena, Germany), high resolution transmission electron microscopy (HR-TEM) (JEOL-JEM 2100 microscope, Tokyo, Japan) operated at 200 keV, and coupled with an electron diffraction X-ray scattering (EDX) analyser. The structure of the PPy homopolymer and PPy-*m*DP/Fe<sub>3</sub>O<sub>4</sub> nanocomposite before and after adsorption was confirmed using Attenuated Total Reflectance Fourier transform infrared with a germanium crystal-attenuated total reflectance Fourier transform infrared microscopy (ATR-FTIR) PerkinElmer Spectrum 100 spectrometer (PerkinElmer, Johannesburg, South Africa). For IR measurements, the frequency range, resolution and number of scans were in the range of 650–4000 cm<sup>-1</sup>, 4 cm<sup>-1</sup> and 10 cm<sup>-1</sup>, respectively. X-ray diffraction (XRD) patterns of the PPy homopolymer and PPy-*m*PD/Fe<sub>3</sub>O<sub>4</sub> nanocomposite before and after the removal of Cr(VI) were obtained using a PANalytical X'Pert PRO-diffractometer (PANalytical, Eindhoven, The Netherlands). The spectra were achieved using the CuK<sub>α</sub> radiation ( $\lambda = 1.5406 \text{ \AA}$ ) at 45 kV/40 mA and 2 $\theta$  values ranging between 5 and 90°. The Brunauer–Emmet–Teller (BET) analysis was performed at a low-temperature N<sub>2</sub> adsorption–desorption technique, using a Micromeritics ASAP 2020 gas adsorption apparatus (Micromeritics, Norcross, USA). The thermal stability of the prepared nanocomposite was studied using a thermogravimetric analyser (TGA) Q500 (TA Instruments, New Castle, USA). Furthermore, the sample was heated from 25 to 800 °C at a heating rate of 10 °C/min and the flow rate of 50 mL/min in air. The magnetic properties of the PPy-*m*PD/Fe<sub>3</sub>O<sub>4</sub> nanocomposite were studied using a vibrating sample magnetometer (VSM, Lakeshore, Westerville, USA) at room temperature and a maximum applied magnetic field of 9.6 kOe. Ion chromatography coupled to inductively coupled plasma mass spectroscopy (IC-ICP-MS) (ThermoFisher Scientific instrumentation, Waltham, USA) was utilised to determine the concentration of Cr(VI) and Cr(III) ions present in the solutions obtained from the effect of the pH experiment. The measurement of Cr(VI) concentrations in solutions after adsorption by the PPy-*m*PD/Fe<sub>3</sub>O<sub>4</sub> nanocomposite was conducted using an ultraviolet-visible (UV-vis) spectrophotometer, (Perkin Elmer, Johannesburg, South Africa).

### 2.4. Batch Adsorption Experiments

Batch adsorption experiments were executed to study the effect of adsorbent dose, solution pH, initial Cr(VI) concentration, temperature and co-existing ions on Cr(VI) adsorption by PPy-*m*PD/Fe<sub>3</sub>O<sub>4</sub> nanocomposite. Different concentrations of Cr(VI) solution were prepared by diluting the 1000 mg/L

Cr(VI) stock solution to evaluate these various parameters. For adsorption equilibrium experiments, a fixed amount of the nanocomposite (0.025 g) was contacted with 50 mL of 100 mg/L Cr(VI) solution in 100 mL plastic bottles in a thermostat shaker agitated for 24 h at a speed of 200 rpm. For pH studies, the pH of Cr(VI) solution was varied from 2.0–11.0 adjusted with HCl and NaOH solutions with 100 mg/L initial Cr(VI) concentration.

The point of zero charge ( $\text{pH}_{\text{pzc}}$ ) of the PPy-*m*PD/Fe<sub>3</sub>O<sub>4</sub> nanocomposite was determined by the pH drift method. To a series of 100 mL plastic bottles, 50 mL of 100 mg/L Cr(VI) was added, and the initial pH ( $\text{pH}_i$ ) was adjusted from 2–11 with 0.1 M HCl or 0.1 M NaOH solutions. To the adjusted pH solutions, 25 mg of PPy-*m*PD/Fe<sub>3</sub>O<sub>4</sub> nanocomposite was added and the suspensions were placed in a thermostat shaker agitated for 24 h at a speed of 200 rpm. After 24 h, the suspensions were separated by filtration, and the final pH values of supernatant liquid were recorded.

The effect of adsorbent dose was carried out by varying the mass of the PPy-*m*PD/Fe<sub>3</sub>O<sub>4</sub> nanocomposite from 0.005–0.05 g. Adsorption isotherms experiments were conducted at 15, 25, 35 and 45 °C to study Cr(VI) removal by the nanocomposite, while varying the concentration of the Cr(VI) from 100 to 600 mg/L.

For adsorption kinetics experiments, solutions with four initial Cr(VI) concentrations (25, 50, 75 and 100 mg/L) were prepared and contacted with PPy-*m*PD/Fe<sub>3</sub>O<sub>4</sub> adsorbent to examine the contact time effect on the removal of Cr(VI). In a typical experiment, the PPy-*m*PD/Fe<sub>3</sub>O<sub>4</sub> nanocomposite (0.5 g) was mixed with 1 L of 100 mg/L Cr(VI) solution at a pH of 2 in a temperature-controlled water bath and an overhead stirrer. The mixture was stirred at 200 rpm with a constant temperature of 25 °C, and a few aliquots (7.0 mL) were taken at selected time intervals. The collected samples were filtered using 0.45 µm cellulose acetate syringe filters, and then they were analysed.

Different ions ( $\text{Cu}^{2+}$ ,  $\text{Zn}^{2+}$ ,  $\text{Co}^{2+}$ ,  $\text{Ni}^{2+}$ ,  $\text{NO}_3^-$ ,  $\text{PO}_4^{3-}$ ,  $\text{SO}_4^{2-}$  and  $\text{Cl}^-$ ) were selected to examine the effect of co-existing ions at different concentrations ranging from 20–100 mg/L in solutions on Cr(VI) removal by the PPy-*m*PD/Fe<sub>3</sub>O<sub>4</sub> nanocomposite. The removal efficiency and the behaviour of the nanocomposite was obtained with the help of the following expressions (Equations (1) and (2)):

$$\% \text{ removal} = \left( \frac{C_o - C_e}{C_o} \right) \times 100 \quad (1)$$

$$q_e = \left( \frac{C_o - C_e}{m} \right) V \quad (2)$$

where  $C_o$  and  $C_e$  represent the initial and equilibrium concentrations of Cr(VI) in mg/L, respectively.  $q_e$  denotes the quantity of Cr(VI) adsorbed at equilibrium/unit mass of PPy-*m*PD/Fe<sub>3</sub>O<sub>4</sub> adsorbent (mg/g). Both where  $m$  (g) and  $V$  (L) represent the mass of the adsorbent and the volume of Cr(VI) solution used, respectively.

Nonlinear and linear forms of the Langmuir and Freundlich isotherm models are presented in the following expressions, respectively, (Equations (3)–(6)) [3].

$$\frac{q_e}{q_m} = \frac{K_L C_e}{1 + K_L C_e} \quad (3)$$

$$q_e = K_F C_e^{1/n} \quad (4)$$

$$\frac{C_e}{q_e} = \frac{1}{q_m K_L} + \frac{C_e}{q_m} \quad (5)$$

$$\ln q_e = \ln K_F + \frac{1}{n} \ln C_e \quad (6)$$

where  $q_m$  (mg/g),  $K_L$  (L/mg),  $K_F$  (mg/g) and  $n$  each represent the Langmuir maximum adsorption capacity, Langmuir constant, Freundlich constant and adsorption intensity, respectively [2,3].

The thermodynamic parameters, such as the Gibbs free energy change ( $\Delta G^0$ ), enthalpy change ( $\Delta H^0$ ) and entropy change ( $\Delta S^0$ ) for the adsorption process can be determined from the relationship of temperature and adsorption isotherms. Particularly,  $\Delta G^0$  can be calculated using Equation (7).

$$\Delta G^0 = -RT \ln K_c \quad (7)$$

To determine the values of  $\Delta S^0$  and  $\Delta H^0$ , a graph of  $\ln K_c$  against  $1/T$  (Figure S1) was plotted according to the following expressions:

$$\ln K_c = \frac{\Delta S^0}{R} - \frac{\Delta H^0}{RT} \quad (8)$$

$$K_c = m \frac{q_e}{C_e} \quad (9)$$

where  $K_c$  (L/mol) is the equilibrium constant which represents the ratio of equilibrium concentration of Cr(VI) adsorbed onto the PPy-*m*PD/Fe<sub>3</sub>O<sub>4</sub> nanocomposite to that in the bulk solution,  $R$  (J/mol/K) is the ideal gas constant,  $T$  (K) is the temperature, and  $m$  (g/L) is the adsorbent dose.

To determine the adsorption rate and other adsorption kinetics parameters, the data obtained was fit to the nonlinear and linear forms of the pseudo-first-order (PFO) and the pseudo-second-order kinetic (PSO) models with the help of the following expressions:

$$\frac{dq_t}{dt} = k_1(q_e - q_t) \quad (10)$$

$$\frac{dq_t}{dt} = k_2(q_e - q_t)^2 \quad (11)$$

$$\ln(q_e - q_t) = \ln q_e - k_1 t \quad (12)$$

$$\frac{t}{q_t} = \frac{1}{k_2 q_e^2} + \frac{1}{q_e} t \quad (13)$$

where  $k_1$  (1/min) represents pseudo-first-order rate (PFOR) constant and  $k_2$  (g/mg.min) denotes the pseudo-second-order rate (PSOR) constant.

### 3. Results and Discussion

#### 3.1. Morphological Characterisations

The morphology and structure of the PPy and its nanocomposite are shown in Figure 1. FE-SEM images are depicted in Figure 1a–c, TEM (Figure 1d,e) and the HR-TEM image in Figure 1f. Figure 1a–c illustrate the PPy and the nanocomposite. As seen in the FE-SEM and TEM images in Figure 1a,d, the PPy homopolymer comprises highly agglomerated spherical-shaped particles, which are similar to those reported by Chen and coworkers [19]. The particle size of the PPy-*m*PD/Fe<sub>3</sub>O<sub>4</sub> nanocomposite depicted in Figure 1b,e are smaller than that of the PPy homopolymer. The presence and distribution of Fe<sub>3</sub>O<sub>4</sub> nanoparticles in the functionalised PPy with *m*PD was observed in the FE-SEM images obtained using the backscatter mode presented in Figure 1c. It can be noticed that the nanoparticles appear as bright spots with an observable agglomerated morphology. The TEM image in Figure 1f depicts lattice fringes possessing an interplanar d-spacing of 0.2983 nm. The obtained d-spacing of 0.2983 nm is assigned to the (220) plane of the cubic spinel structure of Fe<sub>3</sub>O<sub>4</sub> nanoparticles [20]. Figure 2a–e present HR-TEM and elemental mapping images of the PPy-*m*PD/Fe<sub>3</sub>O<sub>4</sub> nanocomposite after the adsorption of Cr(VI). From these images, it was noticed that the Cr ions are adsorbed onto the nanocomposite. This observation confirms the successful incorporation of Fe<sub>3</sub>O<sub>4</sub> nanoparticles into the nanocomposite, and the adsorption of Cr(VI). The corresponding EDX spectrum depicted in Figure 2f shows peaks corresponding to C (0.3 keV), N (0.4 keV), O (0.5 keV), Cl (2.7 keV), Fe (6.5 keV and 7.2 keV) and Cr (5.5 keV and 6 keV).



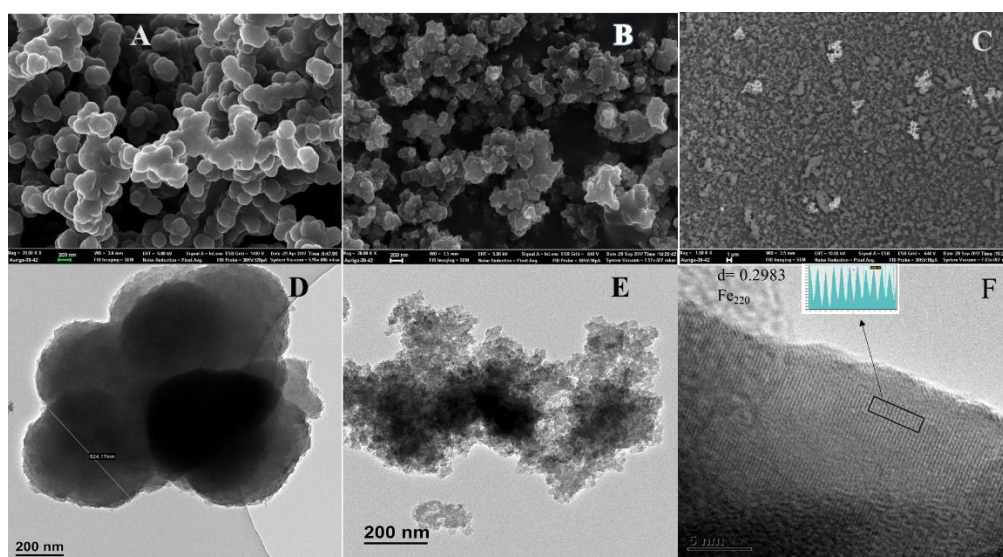


**Figure 1.** Scanning electron microscopy (SEM) images of polypyrrole (PPy) (A) and polypyrrole-*m*-phenyldiamine/Fe<sub>3</sub>O<sub>4</sub> (PPy-*m*PD/Fe<sub>3</sub>O<sub>4</sub>) nanocomposite (B,C); Transmission electron microscopy (TEM) images of PPy (D) and PPy-*m*PD/Fe<sub>3</sub>O<sub>4</sub> nanocomposite (E); High resolution transmission electron microscopy (HR-TEM) of the PPy-*m*PD/Fe<sub>3</sub>O<sub>4</sub> nanocomposite (F). N.B: Field-emission scanning electron microscopy (FE-SEM) image of the nanocomposite carried out in the backscattered mode (C).

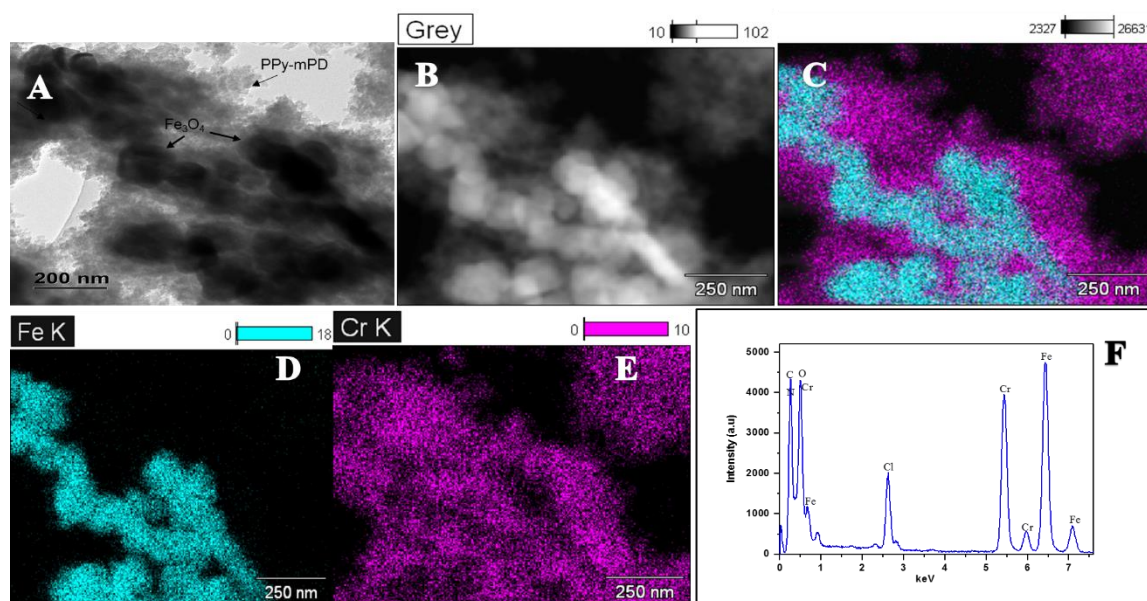


**Figure 2.** (A) HR-TEM images, (B–E) elemental mapping images, and electron diffraction X-ray scattering (EDX) spectra (F) of the PPy-*m*PD/Fe<sub>3</sub>O<sub>4</sub> nanocomposite after Cr(VI) adsorption.

### 3.2. Fourier Transform Infrared Analysis

Fourier transform infrared (FTIR) spectra of PPy and PPy-*m*PD/Fe<sub>3</sub>O<sub>4</sub> nanocomposite, before and after Cr(VI) adsorption, are provided in Figure 3. Figure 3a shows the bands obtained for the PPy homopolymer at 798, 854, 1000, 1190, 1300, 1452 and 1511 cm<sup>-1</sup>, corresponding to the C–H out-of-plane ring deformation of pyrrole, C–H in-plane deformation, N–H in-plane deformation, C–N stretching, C–N ring stretching, as well as the ring stretching mode of C=C [21]. The presence of Fe<sub>3</sub>O<sub>4</sub> nanoparticles in the PPy-*m*PD/Fe<sub>3</sub>O<sub>4</sub> nanocomposite before the adsorption of Cr(VI) is confirmed by the intense band at 520 cm<sup>-1</sup> as shown in Figure 2b. The band at 3180 cm<sup>-1</sup> is attributed to the N–H

stretching vibration of the *m*PD in the nanocomposite. In addition, the vibration band at  $3300\text{ cm}^{-1}$  is associated with the presence of moisture in the nanocomposite [22].

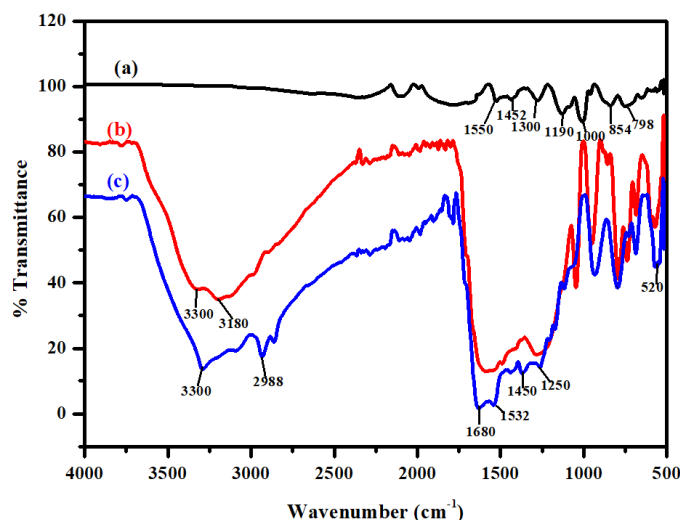


**Figure 3.** Fourier transform infrared (FTIR) spectra of PPy (a), PPy-*m*PD/Fe<sub>3</sub>O<sub>4</sub> nanocomposite before (b) and after (c) Cr(VI) adsorption.

The FTIR spectrum of nanocomposite after Cr(VI) adsorption is given in Figure 2c. It is noticeable that there is a shift in the N–H vibration band appearing at  $3180\text{ cm}^{-1}$  to  $2988\text{ cm}^{-1}$ . The shift is due to electrostatic interaction of  $\text{HCrO}_4^-$  on the PPy-*m*PD/Fe<sub>3</sub>O<sub>4</sub> nanocomposite [23]. Furthermore, the nanocomposite revealed bands at  $1680$ ,  $1532$  and  $1250\text{ cm}^{-1}$ , corresponding to the quinoid imines, benzoid amines and C–N stretching of *m*PD, respectively.

### 3.3. X-ray diffraction, Brunauer–Emmet–Teller, Thermogravimetric Analysis and Vibrating Sample Magnetometer Studies

XRD, BET, TGA and VSM analyses were conducted to support the FTIR findings for the successful synthesis of the nanocomposite, and the results are presented in Figure 4. The XRD analysis was done, and the diffraction patterns of the synthesised PPy, magnetite nanoparticles and the PPy-*m*PD/Fe<sub>3</sub>O<sub>4</sub> nanocomposite prior to and after Cr(VI) adsorption, are given in Figure 4A(a–d). The XRD pattern of the Fe<sub>3</sub>O<sub>4</sub> nanoparticles (Figure 4A(a)) exhibits sharp peaks appearing at  $2\theta = 32.2$ ,  $38.0$ ,  $44.4$ ,  $64.7$ ,  $78.1$  and  $83.5^\circ$ , assigned to the (220), (311), (400), (422), (511) and (440) planes, respectively, indicating the highly crystalline phase purity of the nanoparticles [20]. These results agree well with the HR-TEM results in Figure 1f. Figure 4A(b) shows the XRD pattern of the PPy with a broad peak appearing at  $2\theta = 25^\circ$ , suggesting an amorphous structure of the PPy homopolymer [2]. It was seen that upon the nanocomposite formation (Figure 4A(c)), the patterns shifted to lower  $2\theta$  values as compared to PPy homopolymer and Fe<sub>3</sub>O<sub>4</sub> nanoparticles with the disappearance of peak intensity of the 511 and 440 planes. Furthermore, Figure 4A(d) is the XRD pattern of the PPy-*m*PD/Fe<sub>3</sub>O<sub>4</sub> nanocomposite after Cr(VI) adsorption, which shows the reduction in peak intensity at  $2\theta = 25^\circ$ , indicating the presence of adsorbed Cr(VI) on the surface of the PPy-*m*PD/Fe<sub>3</sub>O<sub>4</sub> nanocomposite [3,6].

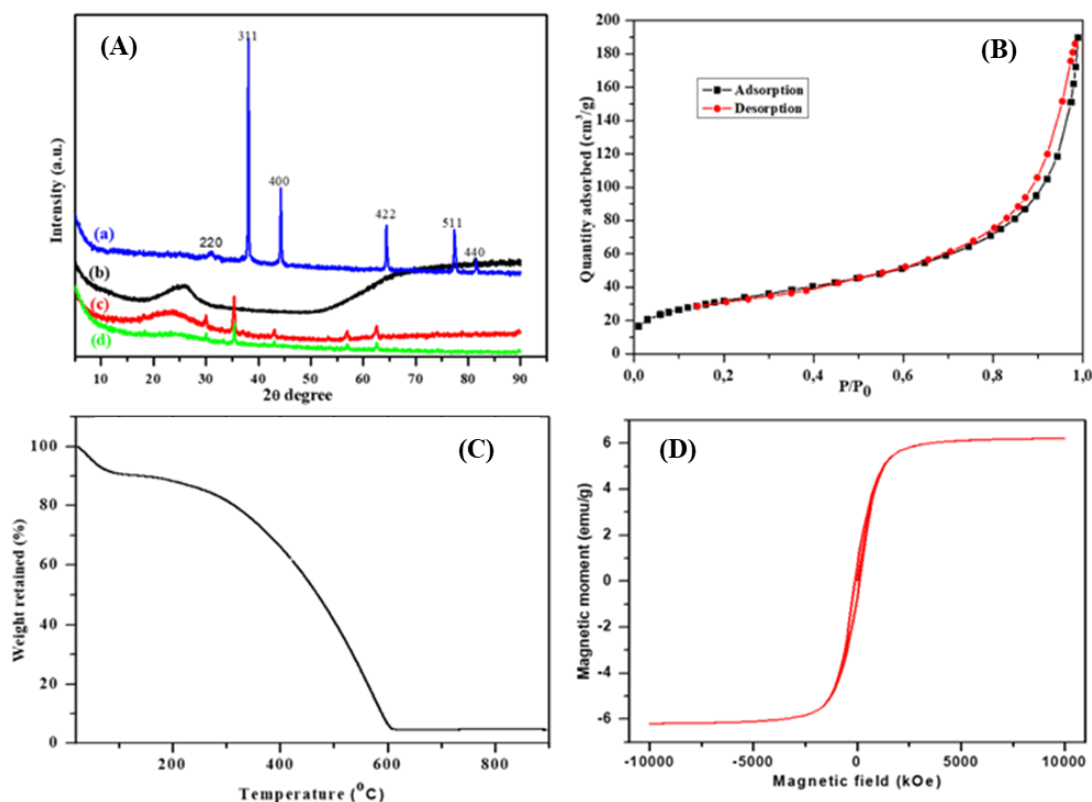


**Figure 4.** X-ray diffraction (XRD) patterns (A) of (a)  $\text{Fe}_3\text{O}_4$  nanoparticles, (b) PPy and PPy-*m*PD/ $\text{Fe}_3\text{O}_4$  nanocomposite before (c) and after (d) Cr(VI) adsorption. Brunauer–Emmet–Teller (BET) spectrum (B), thermogravimetric analysis (TGA) thermogram (C) and vibrating sample magnetometer (VSM) plot (D) of the PPy-*m*PD/ $\text{Fe}_3\text{O}_4$  nanocomposite.

The BET surface area of the PPy-*m*PD/ $\text{Fe}_3\text{O}_4$  nanocomposite was obtained using the  $\text{N}_2$  adsorption/desorption curves, and the results are presented in Figure 4B. It is noticeable that the nanocomposite shows the type IV isotherm hysteresis loop, suggesting the mesoporous nature of the nanocomposite [23]. The BET specific surface area, average pore volume and diameter of the nanocomposite, were found to be  $120.63 \text{ m}^2/\text{g}$ ,  $0.2961 \text{ m}^3/\text{g}$  and  $11.69 \text{ nm}$ , respectively. In another study [2], it was shown that the BET specific surface areas of the PPy and PPy-*m*PD nanocomposites were  $5.3$  and  $183.2 \text{ m}^2/\text{g}$ , respectively. The authors concluded that an addition of *m*PD into the PPy increased the surface area, owing to a reduction in the particle size. In our study, a reduction in the surface area for the PPy-*m*PD/ $\text{Fe}_3\text{O}_4$  nanocomposite may be due to nanoparticles entering or partially blocking some of the PPy-*m*PD nanocomposite pores [6].

The thermal stability of the PPy-*m*PD/ $\text{Fe}_3\text{O}_4$  nanocomposite was studied using TGA, and the result is shown in Figure 4C. It can be seen that the nanocomposite shows the mass loss at  $100 \text{ }^\circ\text{C}$ , due to the release of moisture, and the mass decrease between  $100$ – $200 \text{ }^\circ\text{C}$ , which is attributable to the disintegration of lower molecular weight oligomers that are present [3]. The degradation of the nanocomposite took place from  $140$ – $600 \text{ }^\circ\text{C}$ , implying that below  $140 \text{ }^\circ\text{C}$ , the nanocomposite is thermally stable, and can be used for water purification processes performed at ambient conditions. The percentage weight retained of the  $\text{Fe}_3\text{O}_4$  nanoparticles at the end of the cycle was about  $5.0 \text{ wt } \%$ .

The VSM plot was used to study the magnetic behaviour of the synthesised PPy-*m*PD/ $\text{Fe}_3\text{O}_4$  nanocomposite measured at  $300 \text{ K}$ , and the data are given in Figure 4D. The magnetic hysteresis loop exhibits that the saturation magnetisation ( $M_s$ ) value of the nanocomposite was  $6.6 \text{ emu/g}$ . This value is less than that reported in the literature for the  $\text{Fe}_3\text{O}_4$ /PPy nanocomposite, which might be due to the small amount of  $\text{Fe}_3\text{O}_4$  nanoparticles used for the preparation of the nanocomposite [23]. Again, magnetisation hysteresis of the nanocomposite was close to zero, and this is common for

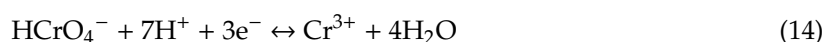


superparamagnetic-based iron oxide nanoparticles, and confirms their superparamagnetic nature of the nanocomposite synthesised in this study [24]. Even though there was a reduction in  $M_s$  value, the nanocomposite still possessed enough magnetic power to be separated by an external magnetic field from aqueous solution after the removal of Cr(VI).

### 3.4. Adsorption Properties

To perform batch adsorption experiments, the effect of adsorbent dose, solution pH, initial Cr(VI) concentration, temperature, and the co-existing ions on Cr(VI) adsorption by PPy-*m*PD/Fe<sub>3</sub>O<sub>4</sub> nanocomposite, were investigated.

The pH of the solution is the most vital parameter to be considered for the adsorption of heavy metal ions, because it affects the surface charge of the adsorbent, as well as the speciation of the metal ions in solution [25]. Figure 5a shows the effect of pH on the removal efficiency of Cr(VI) by the PPy-*m*PD/Fe<sub>3</sub>O<sub>4</sub> nanocomposite. It can be seen that there is a reduction in the removal efficiency of Cr(VI) as the pH was increased from 2.0–11.0. To determine the surface charge of the adsorbent, the point of zero charge (pH<sub>pzc</sub>) was done. The pH<sub>pzc</sub> is simply the pH at which the adsorbent surface has a net charge of zero. It is obtained from the difference between the initial pH<sub>i</sub> and the final pH (pH<sub>f</sub>). The plot of ΔpH as a function of pH<sub>i</sub> is presented in the Supplementary Information (Figure S2) for the determination of pH<sub>pzc</sub> for the PPy-*m*PD/Fe<sub>3</sub>O<sub>4</sub> nanocomposite. From the results, it was observed that the nanocomposite has a pH<sub>pzc</sub> at a pH of 2.3, which correlates well with the pH studies, since the maximum adsorption capacity was obtained at pH 2 and decreased with increasing pH. At pH up to 2–6, the most prevailing Cr(VI) species in solution are the HCrO<sub>4</sub><sup>−</sup> and Cr<sub>2</sub>O<sub>7</sub><sup>2−</sup> oxyanions, which become CrO<sub>4</sub><sup>2−</sup> as the pH increases above 6 [26]. At pH 2, the nitrogen atoms of the amino groups (−NH<sub>2</sub>) on the surface of the nanocomposite are protonated (−NH<sub>3</sub><sup>+</sup>), and attract the negatively-charged Cr(VI) oxyanions. This results in the adsorption of the Cr(VI) anions onto the surface of the PPy-*m*PD/Fe<sub>3</sub>O<sub>4</sub> nanocomposite [26]. The decrease in the removal efficiency of Cr(VI) as the pH rises is due to an increased competition between the hydroxyl (OH<sup>−</sup>) ions and the CrO<sub>4</sub><sup>2−</sup> anions for the active adsorption sites (−NH<sub>3</sub><sup>+</sup>) on the surface of the nanocomposite, and this results in more Coulombic repulsion anions [27]. Speciation studies were carried out using IC-ICP-MS to determine the concentrations of Cr(III) and Cr(VI) in solutions, and the results are given in Figure 5b. From the data given in Figure 3b, it is noticeable that at pH 2, Cr(III) species occur in the solution after Cr(VI) removal. This confirms that the PPy-*m*PD/Fe<sub>3</sub>O<sub>4</sub> nanocomposite has the ability to both adsorb and reduce Cr(VI) to Cr(III). The HCrO<sub>4</sub><sup>−</sup> form which exists at pH 2 has a high redox potential, and is therefore reduced to Cr(III) by the nanocomposite [1,2], as shown in this expression (Equation (14)):



The effect of adsorbent dosage was performed to determine the minimum amount of PPy-*m*PD/Fe<sub>3</sub>O<sub>4</sub> nanocomposite required to remove (% removal) and the adsorption equilibrium ( $q_e$ ) of the Cr(VI) from the solution at pH 2 (100 mg/L, 50 mL). The % removal and  $q_e$  results are presented in Figure 6. By varying the adsorbent dosage (0.005–0.05 g), the minimum amount of nanocomposite required to remove Cr(VI) from aqueous solution entirely was found to be 0.025 g.

Adsorption isotherms are pivotal in studying the interaction between the adsorbent and the adsorbate, as well as to evaluate the maximum capacity of the adsorbent [23]. The temperature effect on Cr(VI) uptake by the PPy-*m*PD/Fe<sub>3</sub>O<sub>4</sub> nanocomposite was conducted at various temperatures (15–45 °C). The adsorption isotherms in Figure 5a show that the adsorption process is temperature-dependent (i.e., endothermic). This behaviour is supported by an increase in equilibrium adsorption capacity with increasing temperature. The obtained adsorption isotherm data were fitted to two isotherm models (Langmuir and Freundlich). It is known that the Freundlich isotherm is a well-known empirical model [28–30], which is not restricted to the formation of a monolayer. Figure 7a,b show the plots obtained from fitting the data to different forms of the isotherm models, and the calculated isotherm

parameters are presented in Table 1. The correlation coefficients ( $R^2$ ) obtained for the linear and nonlinear Langmuir model are 0.99 and 0.95, respectively. In the case of the Freundlich model,  $R^2 = 0.93$  and 0.87 for linear (Figure S3) and nonlinear (Figure 7a) forms, respectively. From the table, it can be observed that the data fitted the Langmuir model better (Figure 7b) than the Freundlich model (Supporting Information). This implies that the surface of the nano-adsorbent is homogeneous (without the inter-reaction amongst adsorbed species), and with all the active adsorption sites equal in energy [2]. Furthermore, the monolayer surface coverage assumed by the Langmuir model can be associated with the electrostatic interaction occurring amongst Cr(VI) ions and the protonated PPy-*m*PD/Fe<sub>3</sub>O<sub>4</sub> [30].

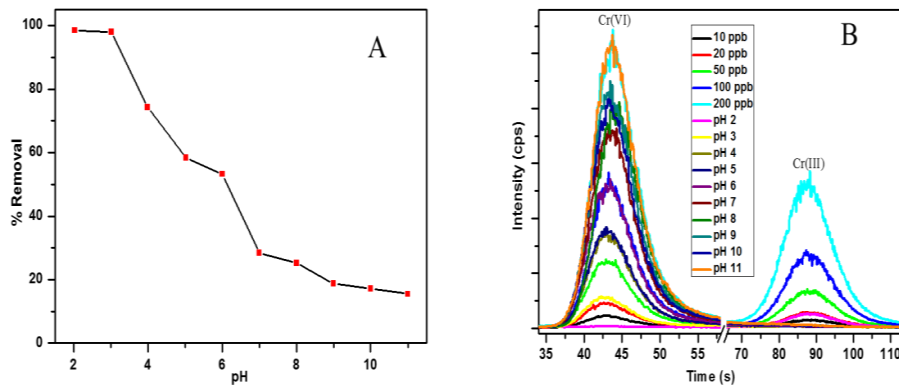


**Figure 5.** The effect of pH on Cr(VI) by adsorbent (A) and IC-ICP-MS chromatograms for analysis of chromium speciation (B) in standard solutions and the solutions obtained from the pH effect experiments.

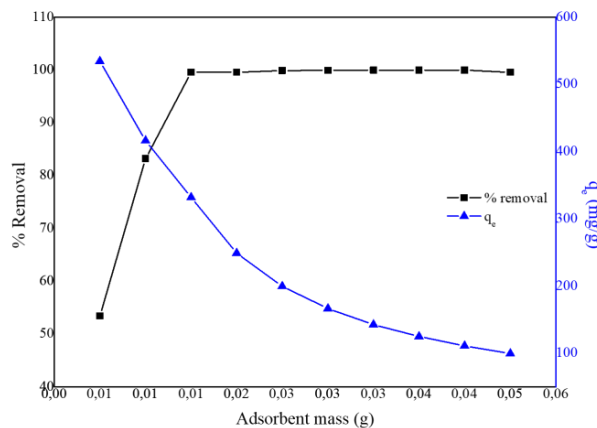


**Figure 6.** Effect of PPy-*m*PD/Fe<sub>3</sub>O<sub>4</sub> adsorbent dose on the removal of Cr(VI) from the solution.

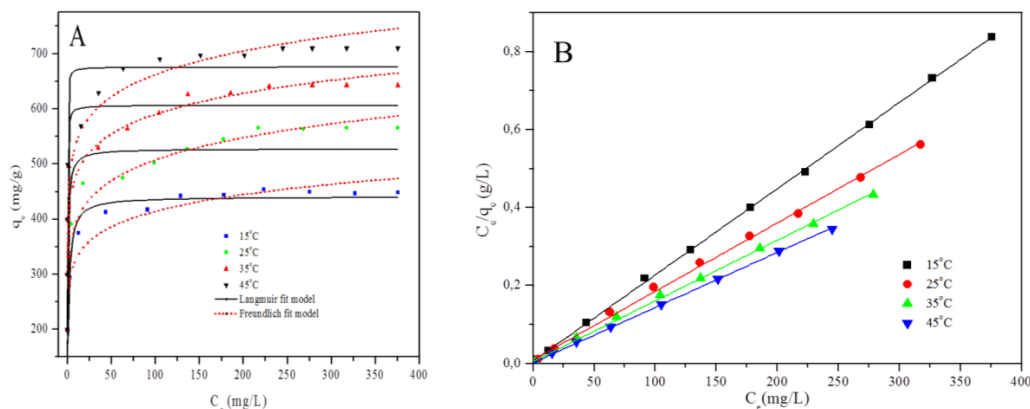


**Figure 7.** Isotherm data to the Langmuir and Freundlich models (A) and Isotherm data to the linear form of the Langmuir model for Cr(VI) adsorption (B) by PPy-*m*PD/Fe<sub>3</sub>O<sub>4</sub> nanocomposite adsorbent.

**Table 1.** Isotherm parameters for Cr(VI) adsorption by PPy-*m*PD/Fe<sub>3</sub>O<sub>4</sub> using both Langmuir and Freundlich models.

Isotherm Model	Temperature			
	15 °C	25 °C	35 °C	45 °C
Langmuir				
Linear				
$q_m$	454.5	555.6	625	714.3
$K_L$	0.338	0.194	0.314	0.583
$R_L$	0.00838	0.01451	0.00902	0.00488
$R^2$	0.9997	0.9982	0.9986	0.9996
Non-linear				
Best-fit values				
$q_m$	440.6	522.4	596.5	661.0
$K_L$	0.7719	1.914	8.046	13.05
Std. Error				
$q_m$	6.038	15.80	15.01	19.06
$K_L$	0.09790	0.5212	1.483	2.537
95% Confidence Intervals				
$q_m$	426.9–454.2	486.6–558.1	562.6–630.5	617.9–704.1
$K_L$	0.5505–0.9934	0.7353–3.093	4.692–11.40	7.317–18.79
Goodness of Fit				
Degrees of Freedom	9	9	9	9
$R^2$	0.9611	0.9536	0.9310	0.9250
Absolute Sum of Squares	2592	6727	15505	24061
Sy.x	16.97	27.34	41.51	51.71
Number of points				
Analysed	11	11	11	11
Freundlich				
Linear				
$K_F$	240.495	287.349	370.369	415.715
$N$	8.46	7.94	9.5	9.18
$R^2$	0.8829	0.9358	0.8536	0.845
Non-linear				
Best-fit values				
$K_F$	259.1	303.1	388.2	435.5
$N$	9.816	8.847	10.76	10.47
Std. Error				
$K_F$	17.73	14.53	21.38	23.13
$N$	1.342	0.7892	1.391	1.319
95% Confidence Intervals				
$K_F$	219.0–299.2	270.3–336.0	339.8–436.6	383.2–487.8
$N$	6.780–12.85	7.062–10.63	7.613–13.91	7.482–13.45
Goodness of Fit				
Degrees of Freedom	9	9	9	9
$R^2$	0.8899	0.8747	0.9052	0.9102
Absolute Sum of Squares	7329	18170	21322	28790
Sy.x	28.54	44.39	48.67	56.56
Number of points				
Analysed	11	11	11	11

Units:  $q_m$ : mg/g,  $K_L$ : L/mg,  $K_F$ : mg/g.

Another important parameter related to the Langmuir model is the dimensionless constant  $R_L$ , which is used to determine whether the adsorption process is favourable or unfavourable. This separation factor was obtained from Equation (15):

$$R_L = \frac{1}{1 + K_L C_0} \quad (15)$$

The  $R_L$  value indicates favourable adsorption for  $0 < R_L < 1$ . The  $R_L$  values in Table 1 are between 0 and 1, and this is an indicative of a favourable adsorption process of Cr(VI). The maximum adsorption capacity of the PPy-*m*PD/Fe<sub>3</sub>O<sub>4</sub> adsorbent for Cr(VI) removal was 555.6 mg/g at 25 °C. This value was higher than the maximum adsorption capacities reported for other magnetic composites

(Table S1) [2,3,9,16–18,23,31–38]. Therefore, the incorporation of  $\text{Fe}_3\text{O}_4$  nanoparticles into PPy-*m*PD ( $q_m = 526.3$  mg/g) did not only have an influence on the magnetic properties, but also increased the maximum adsorption capacity, both of which are preferable for water treatment (as the recovery of the material from treated water will be easier owing to the high magnetic property of the nanocomposite) [3]. Generally, the adsorption capacity increased with an increase in initial metal ions concentration present in the solution [33,34]. This was supported by the thermodynamic properties of the synthesised PPy, the magnetite nanoparticles and the PPy-*m*PD/ $\text{Fe}_3\text{O}_4$  nanocomposite for Cr(VI) adsorption.

Table S2 shows the summary of  $\Delta G^0$ ,  $\Delta H^0$  and  $\Delta S^0$  change values obtained at 15, 25, 35 and 45 °C. The negative values of  $\Delta G^0$  suggest that Cr(VI) adsorption occurs spontaneously at all of the temperatures studied. The negative change in  $\Delta G^0$  becomes more negative with increasing temperature for Cr(VI) adsorption by the PPy-*m*PD/ $\text{Fe}_3\text{O}_4$  nanocomposite, implying the feasibility and spontaneous nature of the adsorption process. The slope and the intercept were used to determine the  $\Delta H^0$  and  $\Delta S^0$  of the adsorption. The positive value of  $\Delta H^0$  confirmed that adsorption of Cr(VI) onto PPy-*m*PD/ $\text{Fe}_3\text{O}_4$  nanocomposite was endothermic [35,39], while the positive value of  $\Delta S^0$  indicates that there is a high affinity between Cr(VI) and PPy-*m*PD/ $\text{Fe}_3\text{O}_4$  nanocomposite.

The effect of contact time on Cr(VI) removal by the PPy-*m*PD/ $\text{Fe}_3\text{O}_4$  nanocomposite adsorbent was investigated with four various Cr(VI) initial concentrations, i.e., 25, 50, 75 and 100 mg/L, and the results are depicted in Figure 8 and Figure S4. The figure demonstrates an increase in Cr(VI) uptake with an increase initial Cr(VI) concentrations. The observed increase in Cr(VI) removal with an increase in concentration is due to a large number of Cr(VI) species available in solution, resulting in more collisions between Cr(VI) ions and the nanocomposite surface in the solution [6].

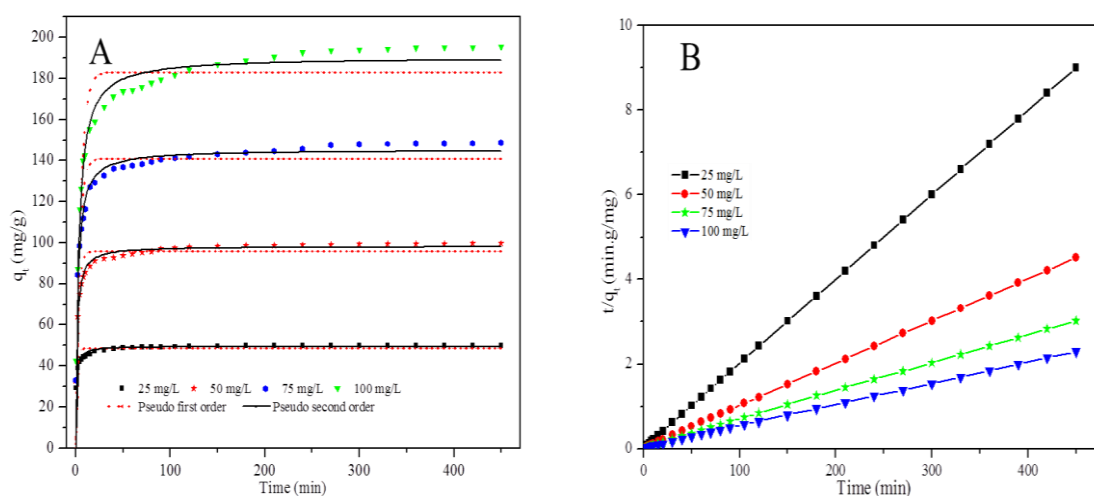


**Figure 8.** Nonlinear fitting of the data to the pseudo-first-order (PFO) and pseudo-second-order (PSO) kinetic models (A) and Fit of the data to the linear form of the PSO kinetic model (B) for Cr(VI) adsorption by the PPy-*m*PD/ $\text{Fe}_3\text{O}_4$  nanocomposite.

Figure 8a shows that the kinetics data fitted the nonlinear PSO kinetic model better than the nonlinear PFO kinetic model. Figure 8b and Figure S4 shows the plots obtained from fitting of the kinetics data to the linear forms of PFO and PSO kinetic models, respectively.

Table S3 shows adsorption kinetic parameters obtained from the linear and nonlinear fitting of the data to the PFO and PSO models. The  $R^2$  values obtained for the linear and nonlinear fittings of the data to the PFO model are lower than those obtained for the PSO kinetic model, suggesting that the adsorption of Cr(VI) onto PPy-*m*PD/ $\text{Fe}_3\text{O}_4$  nanocomposite followed PSO kinetics [25]. Additionally, the obtained  $q_e$  values for the PSO model were comparable to the  $q_e$  values obtained experimentally. The PSOR constants ( $k_2$ ) values decreased with increasing initial Cr(VI) concentration, showing that the rate of Cr(VI) adsorption by the PPy-*m*PD/ $\text{Fe}_3\text{O}_4$  nanocomposite increased as the Cr(VI) initial concentration decreased [7]. Adsorption kinetics data were used to determine the rate-limiting

step (RLS) of Cr(VI) adsorption by the nanocomposite, by fitting the data to the Weber and Morris intra-particle diffusion model (Figure S5). Figure S5 and Table S4 show the  $k_i$  and  $C$  values for three different linear segments obtained for each plot. The results indicate that the three stages control the adsorption process, and are rate limiting at a certain range in time. Furthermore, the larger values of  $k_i$  suggest that film diffusion is faster, and has a more significant role as the RLS [34,36–38]. In addition, temperature-dependent kinetics data were used to calculate the activation energy ( $E_a$ ) for Cr(VI) adsorption by the PPy-*m*PD/Fe<sub>3</sub>O<sub>4</sub> nanocomposite obtained at 15, 25, 35 and 45 °C, and the results are provided in Table S2. The  $E_a$  of the adsorption process can be related to the PSOR constant,  $k_2$  (g/mg/min) by the linearised Arrhenius ( $\ln k_2 = \ln A - \frac{E_a}{RT}$ ),  $T$  is the temperature  $T$  (K),  $A$  (g/mg/min) is the frequency factor,  $R$  denotes the general gas constant (J/mol/K), and  $E_a$  (kJ/mol) is the activation energy. The results show an increase in the rate of Cr(VI) adsorption with an increase in temperature, which gave an  $E_a = 0.0258$  kJ/mol determined from the Arrhenius plot.

The effect of selected ions ( $\text{Cl}^-$ ,  $\text{Co}^{2+}$ ,  $\text{Cu}^{2+}$ ,  $\text{Ni}^{2+}$ ,  $\text{Zn}^{2+}$ ,  $\text{NO}_3^-$ ,  $\text{PO}_4^{3-}$  and  $\text{SO}_4^{2-}$ ) on the Cr(VI) removal by the PPy-*m*PD/Fe<sub>3</sub>O<sub>4</sub> nanocomposite was studied by varying the coexisting ions concentrations in solutions from 20 to 100 mg/L, with the Cr(VI) concentration at  $x$  mg/L. Figure 9 revealed that the four cations ( $\text{Cu}^{2+}$ ,  $\text{Co}^{2+}$ ,  $\text{Zn}^{2+}$ ,  $\text{Ni}^{2+}$ ) had no significant effect on the removal of Cr(VI). This observation was anticipated, since the adsorption of Cr(VI) at pH 2 takes place via anion exchange with dopant  $\text{Cl}^-$  ions in the polymer, and consequently, the PPy-*m*PD/Fe<sub>3</sub>O<sub>4</sub> nanocomposite has no affinity for cations [25,39]. Considering that Cr(VI) exists as an oxyanion, the presence of other anionic compounds may affect its adsorption onto the PPy-*m*PD/Fe<sub>3</sub>O<sub>4</sub> nanocomposite. Hence, the effects of anions ( $\text{Cl}^-$ ,  $\text{NO}_3^-$ ,  $\text{PO}_4^{3-}$  and  $\text{SO}_4^{2-}$ ) were examined to assess competition with Cr(VI) during adsorption. Figure 9 again showed that when the concentration of anions increases to 100 mg/L, there was a slight decrease of  $\approx 3\%$  in the removal of Cr(VI) by PPy-*m*PD/Fe<sub>3</sub>O<sub>4</sub> nanocomposite, due to the  $\text{SO}_4^{2-}$  ions. Even though high concentration of  $\text{SO}_4^{2-}$  existed, the removal of Cr(VI) by the PPy-*m*PD/Fe<sub>3</sub>O<sub>4</sub> nanocomposite was still not hindered significantly. The insignificant effect of low affinity ligands  $\text{Cl}^-$  and  $\text{NO}_3^-$  on Cr(VI) removal by the PPy-*m*PD/Fe<sub>3</sub>O<sub>4</sub> nanocomposite may be because these ligands only form weak outer sphere complexes with binding sites on the adsorbents [26].  $\text{SO}_4^{2-}$  has the ability to form both inner and outer sphere complexes, but as a result of its high hydration energy, as compared to that of Cr(VI), and therefore does not affect the removal of Cr(VI) by the PPy-*m*PD/Fe<sub>3</sub>O<sub>4</sub> nanocomposite [17,18]. The high selective behaviour of the PPy-*m*PD/Fe<sub>3</sub>O<sub>4</sub> nanocomposite towards Cr(VI) may be attributed to the ability of PPy to reduce toxic Cr(VI) to less toxic Cr(III), because of a high positive redox potential of  $\text{HCrO}_4^-$  anions, the main form of Cr(VI) in solutions at low pH [3].

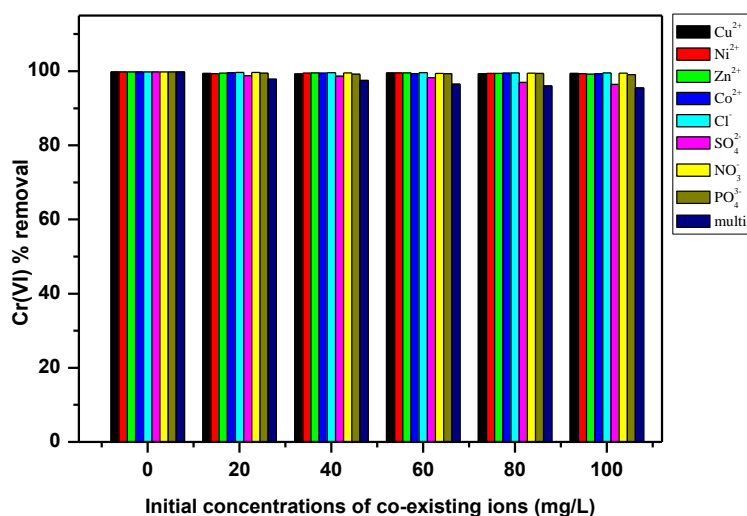
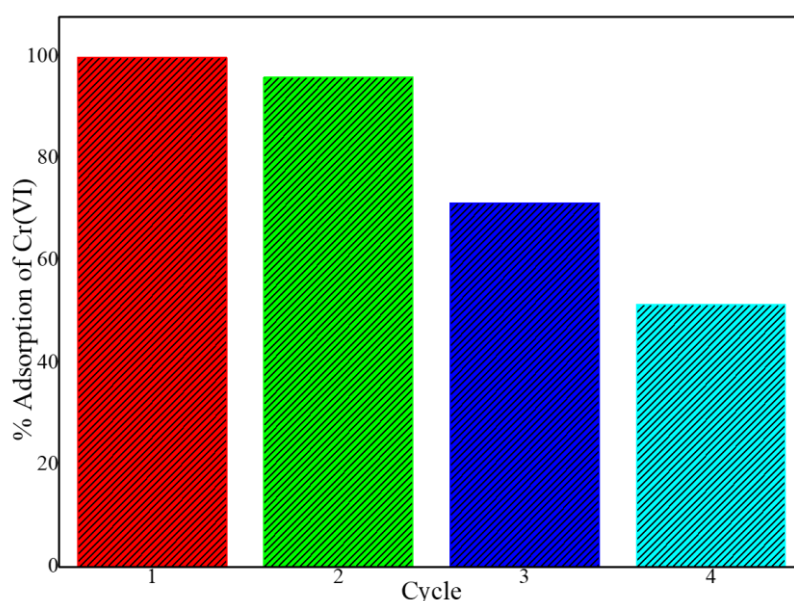


Figure 9. Effect of coexisting ions on Cr(VI) adsorption by the PPy-*m*PD/Fe<sub>3</sub>O<sub>4</sub> nanocomposite.



The regeneration and reusability of adsorbents are important aspects to consider for the economic sustainability of water purification processes. The potential to reuse the PPy-*m*PD/Fe<sub>3</sub>O<sub>4</sub> nanocomposite was assessed by conducting four consecutive adsorption–desorption–regeneration cycles. For the desorption of Cr(VI) from the nanocomposite, an NH<sub>4</sub>OH solution of 0.1 M was used, followed by regeneration using 2 M HCl solution before being used for the next cycle. The results in Figure 10 showed that the PPy-*m*PD/Fe<sub>3</sub>O<sub>4</sub> nanocomposite could be used for two consecutive cycles without a significant reduction in the adsorption capacity, as the removal efficiency was still above 90% in the second cycle. In the third and the fourth cycles, 70% and 50% Cr(VI) removal efficiency by the PPy-*m*PD/Fe<sub>3</sub>O<sub>4</sub> nanocomposite was obtained, respectively. This may be attributed to an overoxidation of the PPy-*m*PD/Fe<sub>3</sub>O<sub>4</sub> nanocomposite, which caused the deterioration of the polymer, and therefore reduced the adsorption sites available for Cr(VI) [26]. From these findings, it must be stated that this is only preliminary desorption research, and they should be continued to find a better desorption–regeneration procedure to prove the sorbent to be useful in practice.



**Figure 10.** Adsorption cycles for Cr(VI) removal by the PPy-*m*PD/Fe<sub>3</sub>O<sub>4</sub> nanocomposite.

#### 4. Conclusions

A novel magnetic PPy-*m*PD/Fe<sub>3</sub>O<sub>4</sub> nanocomposite with a saturation magnetisation of 6.6 emu/g was synthesised for the removal of Cr(VI) from aqueous solution. The adsorption isotherms were obtained at temperatures (15–45 °C) and varying the Cr(VI) initial concentration (100–600 mg/L). The adsorption isotherm data obeyed the Langmuir isotherm model, and a higher Langmuir maximum adsorption capacity of 555.6 mg/g was obtained for Cr(VI) removal by the adsorbent at pH 2 and 25 °C. The PPy-*m*PD/Fe<sub>3</sub>O<sub>4</sub> nanocomposite showed high selectivity towards Cr(VI) adsorption, since the presence of competing ions in solution had no significant effect. Based on the previous results, it can be concluded that the ability to synthesise a magnetic PPy-*m*PD/Fe<sub>3</sub>O<sub>4</sub> nanocomposite containing an increased number of amine functional groups as a very low cost and super-adsorbent material for heavy metal ions was effectively achieved. Thus, due to the high adsorption capacity and selectivity for Cr(VI), the PPy-*m*PD/Fe<sub>3</sub>O<sub>4</sub> nanocomposite is a potential adsorbent for Cr(VI) removal from industrial wastewater.

**Supplementary Materials:** The following are available online at <http://www.mdpi.com/2073-4360/12/3/679/s1>, Figure S1: Plot to obtain the thermodynamic parameters for Cr(VI) adsorption by the PPy-*m*PD/Fe<sub>3</sub>O<sub>4</sub> nanocomposite, Figure S2: The point of the zero charge of the PPy-*m*PD/Fe<sub>3</sub>O<sub>4</sub> nanocomposite, Figure S3: Linear fit of temperature effect data to Freundlich isotherm model for the PPy-*m*PD/Fe<sub>3</sub>O<sub>4</sub> nanocomposite,

Figure S4: Linear fit of pseudo second order kinetic model for Cr(VI) adsorption by the PPy-*m*PD/Fe<sub>3</sub>O<sub>4</sub> nanocomposite, Figure S5: Plots obtained for the intra-particle diffusion (IPD) model for Cr(VI) adsorption by the PPy-*m*PD/Fe<sub>3</sub>O<sub>4</sub> nanocomposite, Table S1: Adsorption capacity of the PPy-*m*PD/Fe<sub>3</sub>O<sub>4</sub> nanocomposite adsorbent, studied in comparison to other adsorbents reported in the literature for the removal of Cr(VI) from solution, Table S2: Thermodynamic values for Cr(VI) adsorption by the PPy-*m*PD/Fe<sub>3</sub>O<sub>4</sub> nanocomposite, Table S3: Kinetics parameters of Cr(VI) adsorption by the PPy-*m*PD/Fe<sub>3</sub>O<sub>4</sub> nanocomposite, Table S4: Intra-particle diffusion model parameters of Cr(VI) adsorption by the PPy-*m*PD/Fe<sub>3</sub>O<sub>4</sub> nanocomposite.

**Author Contributions:** Conceptualisation, K.D.M., A.M. and M.J.H.; Formal analysis, T.C.M., A.M., N.H.K.; Funding acquisition, K.D.M. and M.J.H.; Methodology, T.C.M., N.H.K. and A.M.; Project administration, M.J.H., and K.D.M.; Supervision, M.J.H. and K.D.M.; Writing—Original draft, T.C.M., K.E.R., K.D.M., N.H.K., L.M.K.-S. and M.J.H. All authors have read and agreed to the published version of the manuscript.

**Funding:** This research was supported by the National Research Foundation under Thuthuka program (UIDs. 99166, 108933, 117727 and 118113), University of Limpopo (Research Development Grants Q313, R202, R232, and R355) and Sasol Inzalo Foundation, South Africa.

**Conflicts of Interest:** The authors declare no conflict of interest.

## References

- Wang, Z.; Shen, Q.; Xue, J.; Jia, H.; Xue, B.; Liu, X.; Qi, L. Annealing temperature effect on 3D hierarchically porous NiO/Ni for removal of trace hexavalent chromium. *Mater. Chem. Phys.* **2020**, *240*, 122140. [[CrossRef](#)]
- Hato, M.J.; Maponya, T.C.; Ramohlola, K.E.; Modibane, K.D.; Maity, A.; Monama, G.R.; Makgopa, K.; Bello, A. Polymer-Based magnetic nanocomposites for the removal of highly toxic hexavalent chromium from aqueous solutions. In *Advanced Nanostructured Materials for Environmental Remediation, Environmental Chemistry for a Sustainable World*; Naushad, M., Rajendran, S., Gracia, F., Eds.; Springer: Cham, Switzerland, 2019; Volume 25, pp. 189–227.
- Kera, N.H.; Bhaumik, M.; Pillay, K.; Ray, S.S.; Maity, A. m-Phenylenediamine-modified polypyrrole as an efficient adsorbent for removal of highly toxic hexavalent chromium in water. *Mater. Today Commun.* **2018**, *15*, 153–164. [[CrossRef](#)]
- Yuan, Z.; Cheng, X.; Zhong, L.; Wu, R.; Zheng, Y. Preparation, characterization and performance of an electrospun carbon nanofiber mat applied in hexavalent chromium removal from aqueous solution. *J. Environ. Sci.* **2019**, *77*, 75–84. [[CrossRef](#)] [[PubMed](#)]
- Shaban, M.; Abukhadra, M.R.; Khan, A.A.P. Removal of Congo red, methylene blue and Cr(VI) ions from water using natural serpentine. *J. Taiwan Inst. Chem. Eng.* **2018**, *82*, 102–116. [[CrossRef](#)]
- Wang, J.; Pan, K.; He, Q.; Cao, B. Polyacrylonitrile/polypyrrole core/shell nanofiber mat for the removal of hexavalent chromium from aqueous solution. *J. Hazard. Mater.* **2013**, *244*, 121–129. [[CrossRef](#)]
- Cui, L.; Wang, Y.; Gao, L.; Hu, L.; Yan, L.; Wei, Q.; Du, B. EDTA functionalized magnetic graphene oxide for removal of Pb(II), Hg(II) and Cu(II) in water treatment: Adsorption mechanism and separation property. *Chem. Eng. J.* **2015**, *281*, 1–10. [[CrossRef](#)]
- Bhaumik, M.; Agarwal, S.; Gupta, V.K.; Maity, A. Enhanced removal of Cr(VI) from aqueous solutions using polypyrrole wrapped oxidized MWCNTs nanocomposites adsorbent. *J. Colloid Interface Sci.* **2016**, *470*, 257–267. [[CrossRef](#)]
- Bhaumik, M.; Maity, A.; Srinivasu, V.V.; Onyango, M.S. Enhanced removal of Cr(VI) from aqueous solution using polypyrrole/Fe<sub>3</sub>O<sub>4</sub> magnetic nanocomposite. *J. Hazard. Mater.* **2011**, *190*, 381–390. [[CrossRef](#)]
- Horst, M.F.; Alvarez, M.; Lassalle, V.L. Removal of heavy metals from wastewater using magnetic nanocomposites: Analysis of the experimental conditions. *J. Sep. Sci. Technol.* **2016**, *51*, 550–563. [[CrossRef](#)]
- Can, M.M.; Firat, T.; Özcan, Ş. Interparticle interaction effects on magnetic behaviours of hematite hematite ( $\alpha$ -Fe<sub>2</sub>O<sub>3</sub>) nanoparticles. *Phys. B* **2011**, *406*, 2483–2487. [[CrossRef](#)]
- Can, M.M.; Coşkun, M.; Firat, T. A comparative study of nanosized iron oxide particles; magnetite (Fe<sub>3</sub>O<sub>4</sub>), maghemite ( $\gamma$ -Fe<sub>2</sub>O<sub>3</sub>) and hematite ( $\alpha$ -Fe<sub>2</sub>O<sub>3</sub>), using ferromagnetic resonance. *J. Alloys Compd.* **2012**, *542*, 241–247. [[CrossRef](#)]
- Liu, J.; Dai, C.; Hu, Y. Aqueous aggregation behaviour of citric acid coated magnetite nanoparticles: Effects of pH, cations, anions, and humic acid. *Environ. Res.* **2018**, *161*, 49–60. [[CrossRef](#)] [[PubMed](#)]
- Ilankoon, N. Use of iron oxide magnetic nanosorbents for Cr(VI) removal from aqueous solutions: A review. *Int. J. Eng. Res. Appl.* **2014**, *4*, 55–63.

15. Kumar, S.; Nair, R.R.; Pillai, P.B.; Gupta, S.N.; Iyengar, M.A.R.; Sood, A.K. Graphene oxide-MnFe<sub>2</sub>O<sub>4</sub> magnetic nanohybrids for efficient removal of lead and arsenic from water. *ACS Appl. Mater. Interfaces* **2014**, *6*, 17426–17436. [[CrossRef](#)]
16. Shen, H.; Pan, S.; Zhang, Y.; Huang, X.; Gong, H. A new insight on the adsorption mechanism of amino-functionalized nano-Fe<sub>3</sub>O<sub>4</sub> magnetic polymers in Cu(II), Cr(VI) co-existing water system. *Chem. Eng. J.* **2012**, *183*, 180–191. [[CrossRef](#)]
17. Ballav, N.; Choi, H.J.; Mishra, S.B.; Maity, A. Synthesis, characterization of Fe<sub>3</sub>O<sub>4</sub>@glycine doped polypyrrole magnetic nanocomposites and their potential performance to remove toxic Cr(VI). *J. Ind. Eng. Chem.* **2014**, *20*, 4085–4093. [[CrossRef](#)]
18. Wang, H.; Yuan, X.; Wu, Y.; Chen, X.; Leng, L.; Wang, H.; Li, H.; Zeng, G. Facile synthesis of polypyrrole decorated reduced graphene oxide-Fe<sub>3</sub>O<sub>4</sub> magnetic composites and its application for the Cr(VI) removal. *Chem. Eng. J.* **2015**, *262*, 597–606. [[CrossRef](#)]
19. Chen, H.-C.; Chang, C.-C.; Yang, K.-H.; Mai, F.-D.; Tseng, C.-L.; Chen, L.-Y.; Hwang, B.-J.; Liu, Y.-H. Polypyrrole electrode with a greater electroactive surface electrochemically polymerized in plasmon-activated water. *J. Taiwan. Inst. Chem. Eng.* **2018**, *82*, 252–260. [[CrossRef](#)]
20. Fatima, H.; Lee, D.-H.; Yoon, H.J.; Kim, K.-S. Shape-Controlled synthesis of magnetic Fe<sub>3</sub>O<sub>4</sub> nanoparticles with different precursors and capping agents. *RCS Adv.* **2018**, *8*, 22917–22923. [[CrossRef](#)]
21. Mthombeni, N.H.; Mbakop, S.; Ochieng, S.; Onyango, M.S. Vanadium (V) adsorption isotherms and kinetics using polypyrrole coated magnetized natural zeolite. *J. Taiwan. Inst. Chem. Eng.* **2016**, *66*, 172–180. [[CrossRef](#)]
22. Tang, L.; Fang, Y.; Pang, Y.; Zeng, G.; Wang, J.; Zhou, Y.; Deng, Y.; Yang, G.; Cai, Y.; Chen, J. Synergistic adsorption and reduction of hexavalent chromium using highly uniform polyaniline-magnetic mesoporous silica composite. *Chem. Eng. J.* **2014**, *254*, 302–312. [[CrossRef](#)]
23. Sun, Y.; Yu, F.; Li, C.; Dai, X.; Ma, J. Nano-/micro-confined water in graphene hydrogel as superadsorbents for water purification. *Nano Micro Lett.* **2020**, *12*, 2. [[CrossRef](#)]
24. Zhen, G.; Muir, B.W.; Moffat, B.A.; Harbour, P.; Murray, K.S.; Moubaraki, B.; Suzuki, K.; Madsen, I.; Agron-Olshina, N.; Waddington, L.; et al. Comparative study of the magnetic behavior of spherical and cubic superparamagnetic iron oxide nanoparticles. *J. Phys. Chem. C* **2010**, *115*, 327–334. [[CrossRef](#)]
25. Liu, C.; Liu, H.; Xiong, T.; Xu, A.; Pan, B.; Tang, K. Graphene oxide reinforced alginate/PVA double network hydrogels for efficient dye removal. *Polymers* **2018**, *10*, 835. [[CrossRef](#)] [[PubMed](#)]
26. Bhaumik, M.; Maity, A.; Srinivasu, V.V.; Onyango, M.S. Removal of hexavalent chromium from aqueous solution using polypyrrole-polyaniline nanofibers. *Chem. Eng. J.* **2012**, *181–182*, 323–333. [[CrossRef](#)]
27. Shahid, M.; Shamshad, S.; Rafiq, M.; Khalid, S.; Bibi, I.; Niazi, K.N.; Dumat, C.; Rashid, M.I. Chromium speciation, bioavailability, uptake, toxicity and detoxification in soil-plant system: A review. *Chemosphere* **2017**, *178*, 513–533. [[CrossRef](#)]
28. Bayazit, Ş.S.; Kerkez, Ö. Hexavalent chromium adsorption on superparamagnetic multi-wall carbon nanotubes and activated carbon composites. *Chem. Eng. Res. Des.* **2014**, *92*, 2725–2733. [[CrossRef](#)]
29. Freundlich, H.M.F. Over the adsorption in solution. *J. Phys. Chem.* **1906**, *57*, 385–470.
30. Salam, M.A. Preparation and characterization of chitin/magnetite/multiwalled carbon nanotubes magnetic nanocomposite for toxic hexavalent chromium removal from solution. *J. Mol. Liq.* **2017**, *233*, 197–202. [[CrossRef](#)]
31. Elfeky, S.A.; Mahmoud, S.E.; Youssef, A.F. Applications of CTAB modified magnetic nanoparticles for removal of chromium (VI) from contaminated water. *J. Adv. Res.* **2017**, *8*, 435–443. [[CrossRef](#)]
32. Hou, T.; Kong, L.; Guo, X.; Wu, Y.; Wang, F.; Wen, Y.; Yang, H. Magnetic ferrous-doped graphene for improving Cr(VI) removal. *Mater. Res. Express* **2016**, *3*, 1–8. [[CrossRef](#)]
33. Zhang, Y.; Chi, H.; Zhang, W.; Sun, Y.; Liang, Q.; Gu, Y.; Jing, R. Highly efficient adsorption of copper ions by a PVP-reduced graphene oxide based on a new adsorption mechanism. *Nano Micro Lett.* **2014**, *6*, 80–87. [[CrossRef](#)]
34. Bhaumik, M.; McCrindle, R.; Maity, A. Efficient removal of Congo red from aqueous solutions by adsorption onto interconnected polypyrrole-polyaniline nanofibers. *Chem. Eng. J.* **2013**, *228*, 506–515. [[CrossRef](#)]
35. Guo, X.; Du, B.; Wei, Q.; Yang, J.; Hu, L.; Yan, L.; Xu, W. Synthesis of amino functionalized magnetic graphenes composite material and its application to remove Cr(VI), Pb(II), Hg(II), Cd(II) and Ni(II) from contaminated water. *J. Hazard. Mater.* **2014**, *278*, 211–220. [[CrossRef](#)]
36. Zhao, Y.G.; Shen, H.Y.; Pan, S.D.; Hu, M.Q. Synthesis, characterization and properties of ethylenediamine-functionalized Fe<sub>3</sub>O<sub>4</sub> magnetic polymers for removal of Cr(VI) in wastewater. *J. Hazard. Mater.* **2010**, *182*, 295–302. [[CrossRef](#)]

37. Fang, X.B.; Fang, Z.; Tsang, P.K.E. Selective adsorption of Cr(VI) from aqueous solution by EDA-Fe<sub>3</sub>O<sub>4</sub> nanoparticles prepared from steel pickling waste liquor. *Appl. Surf. Sci.* **2014**, *314*, 655–662. [[CrossRef](#)]
38. Wang, W.; Cai, K.; Wu, X.; Shao, X.; Yang, X. A novel poly(m-phenylenediamine)/reduced graphene oxide/nickel ferrite magnetic adsorbent with excellent removal ability of dyes and Cr(VI). *J. Alloys Compd.* **2017**, *722*, 532–543. [[CrossRef](#)]
39. Wang, N.; Ouyang, X.-K.; Yang, L.-Y.; Omer, A.M. Fabrication of a magnetic cellulose nanocrystal/metal-organic framework composite for removal of Pb(II) from water. *ACS Sustain. Chem. Eng.* **2017**, *5*, 10447–10458. [[CrossRef](#)]



© 2020 by the authors. Licensee MDPI, Basel, Switzerland. This article is an open access article distributed under the terms and conditions of the Creative Commons Attribution (CC BY) license (<http://creativecommons.org/licenses/by/4.0/>).